

---

This is an electronic reprint of the original article.  
This reprint may differ from the original in pagination and typographic detail.

Xi, Fugang; Yang, He; Khayrudinov, Vladislav; He, Yuhang; Haggren, Tuomas; Zhou, Yixuan; Lipsanen, Harri; Sun, Zhipei; Xu, Xinlong

**Enhanced terahertz emission from mushroom-shaped InAs nanowire network induced by linear and nonlinear optical effects**

*Published in:*  
Nanotechnology

*DOI:*  
[10.1088/1361-6528/ac3948](https://doi.org/10.1088/1361-6528/ac3948)

Published: 19/02/2022

*Document Version*  
Peer-reviewed accepted author manuscript, also known as Final accepted manuscript or Post-print

*Please cite the original version:*  
Xi, F., Yang, H., Khayrudinov, V., He, Y., Haggren, T., Zhou, Y., Lipsanen, H., Sun, Z., & Xu, X. (2022). Enhanced terahertz emission from mushroom-shaped InAs nanowire network induced by linear and nonlinear optical effects. *Nanotechnology*, 33(8), Article 085207. <https://doi.org/10.1088/1361-6528/ac3948>

---

This material is protected by copyright and other intellectual property rights, and duplication or sale of all or part of any of the repository collections is not permitted, except that material may be duplicated by you for your research use or educational purposes in electronic or print form. You must obtain permission for any other use. Electronic or print copies may not be offered, whether for sale or otherwise to anyone who is not an authorised user.

# Enhanced Terahertz Emission from Mushroom-Shaped InAs Nanowire Network Induced by Linear and Nonlinear Optical Effects

Fugang Xi<sup>1</sup>, He Yang<sup>2,3</sup>, Vladislav Khayrudinov<sup>3</sup>, Yuhang He<sup>1</sup>, Tuomas Haggren<sup>3</sup>, Yixuan Zhou<sup>1,\*</sup>, Harri Lipsanen<sup>3</sup>, Zhipei Sun<sup>3,\*</sup>, and Xinlong Xu<sup>1,\*</sup>

<sup>1</sup>Shaanxi Joint Lab of Graphene, State Key Laboratory of Photoelectric Technology and Functional Materials, International Collaborative Center on Photoelectric Technology and Nano Functional Materials, Institute of Photonics & Photon-Technology, School of Physics, Northwest University, Xi'an 710127, China.

<sup>2</sup>Summa Semiconductor Oy, Micronova, Espoo FI-00076, Finland

<sup>3</sup>Department of Electronics and Nanoengineering, Aalto University, Espoo, P.O. Box 13500, FI-00076, Finland.

E-mail: yxzhou@nwu.edu.cn, zhipei.sun@aalto.fi, and xlxuphy@nwu.edu.cn

Received xxxxxx

Accepted for publication xxxxxx

Published xxxxxx

## Abstract

The development of powerful terahertz (THz) emitters is the cornerstone for future THz applications, such as communication, medical biology, non-destructive inspection, and scientific research. Here, we report the THz emission properties and mechanisms of mushroom-shaped InAs nanowire (NW) network using linearly polarized laser excitation. By investigating the dependence of THz signal to the incidence pump light properties (e.g., incident angle, direction, fluence, and polarization angle), we conclude that the THz wave emission from the InAs NW network is induced by the combination of linear and nonlinear optical effects. The former is a transient photocurrent accelerated by the photo-Dember field, while the latter is related to the resonant optical rectification effect. Moreover, the *p*-polarized THz wave emission component is governed by the linear optical effect with a proportion of ~85% and the nonlinear optical effect of ~15%. In comparison, the *s*-polarized THz wave emission component is mainly decided by the nonlinear optical effect. The THz emission is speculated to be enhanced by the localized surface plasmon resonance absorption of the In droplets on top of the NWs. This work verifies the nonlinear optical mechanism in the THz generation of semiconductor NWs and provides an enlightening reference for the structural design of powerful and flexible THz surface and interface emitters in transmission geometry.

Keywords: terahertz emitter, InAs, nanowire, resonant optical rectification, photo-Dember effect

---

## 1. Introduction

Due to the increasing demand to explore the terahertz (THz) spectroscopy for applications in communication [1, 2], medical biology [3, 4], non-destructive inspection [5, 6], and

scientific research [7-9], the requirement for efficient, low-cost, and miniaturized THz sources becomes more and more urgent. THz generation from the surface and interface of semiconductors under ultrafast laser excitation is an essential and extensively used method to obtain THz waves for coherent detection in THz time-domain spectroscopy [10-13]. Especially, enhanced THz emission is critical to promote THz imaging by shortening the acquisition time [14]. Compared with the THz photoconductive antenna, the direct use of semiconductors as THz surface emitters is more convenient and flexible. However, there are still some disadvantages restricting the promotion of the THz surface emission. For example, without using external bias and magnetic field, InAs crystal has been used as one of the most robust single semiconductor THz emitters. However, the THz emission efficiency of InAs crystal is only  $\sim 10^{-5}$  [15]; the THz emission from InAs crystal is easy to saturate because of the Fresnel coupling effect [16]; further, InAs crystal is generally used in a reflection excitation geometry due to the high reflectivity to the THz radiation while the transmitted signal is small enough to be ignored [17].

Structurally controlled semiconductors are an accessible and practical method to improve their THz emission performance. For example, nanowires (NWs) have shown electrical and optical properties due to their unique one-dimensional structure [18-20]. As a THz emission material, semiconductor NWs have attracted great research attention because their low dimensional structure and large surface-to-volume ratio can break through the total-internal reflection limitation of the THz radiation generated by dipole radiation in bulk materials [21, 22], thus increasing the THz emission efficiency. Moreover, NWs have tunable length, diameter, directionality, and density so that the THz emission properties can be further adjusted. Therefore, THz emission from many semiconductor NWs have been demonstrated, such as Si [23], Ge [24], GaN [25], GaAs [22, 26], InP [27], Bi<sub>2</sub>Te<sub>2</sub>Se [28] and AlGaAs [29]. Particularly, several works have intensively reported the THz emission phenomena from InAs NWs. In 2011, Seletskiy *et al.* first observed the THz emission from an InAs NW array and found the THz radiation amplitude was only twice smaller than that of an InAs bulk crystal. Considering the fill factor of the NWs, the THz radiation power efficiency was  $\sim 15$  times higher than that of InAs bulk crystals [30]. After, Erhard *et al.* and Arlauskas *et al.* have further reported the enhanced THz emission efficiency of InAs NWs and attribute the THz emission mechanism to the photo-Dember effect [31, 32]. Recently, there is a report on the influence of the excitation laser polarization on the THz generation mechanisms for directions parallel and perpendicular to the NWs [33].

There are at least three key issues that need to be solved for the development of InAs NW-based THz sources: Firstly, although the reported THz emission efficiency of InAs NWs is higher than that of bulk crystals, the total THz emission amplitude of NWs is still lower than that of bulk crystals [30, 32]. It suggests that InAs NWs in a reflection excitation

geometry are still not better than bulk crystals for THz emission. Instead, constructing a transmission-probable sample can take advantage of the low-dimensional structure to break through the transmission limitation of bulk crystals. Secondly, there are different techniques for the preparation of InAs NWs. Compared with catalyst-free methods [32, 33], metal-catalyzed NW growth is generally more convenient and cheaper. Moreover, the probable interface effect between metal catalysts and NWs, and the localized surface plasmon resonance in the metal catalysts [34-36], could also be used to enhance the THz emission. Thirdly, it is well known that the THz emission from InAs crystals is related to the polarization angle of the excitation laser and the azimuth angle of the sample [16, 37, 38] because of the significant impact of the second-order nonlinear optical effect on the THz generation mechanism. However, the nonlinear optical mechanism for the THz generation from InAs NWs has not been clarified.

In this paper, the InAs NW network was prepared on quartz substrate by the metalorganic vapor phase epitaxy method. The short length of  $\sim 0.8 \mu\text{m}$  of the NWs could have less impact on the THz generation by dipole radiation on both the reflection and transmission directions. The quartz substrate has neither THz emission nor absorption. Because NWs are short, the single NW looks like a mushroom, including the In droplet catalyst. Under a linearly polarized 800 nm femtosecond laser excitation, the THz amplitude emitted by the InAs NW network is 1.5 times larger than that of a (100) GaAs crystal. By investigating the influence of the incident angle and direction of the excitation laser on the THz signal, the possible Schottky field between In and InAs is excluded. The THz dipole radiation is attributed to the linear optical effect with a transient photocurrent induced by the photo-Dember effect. The pump fluence dependence of THz amplitude suggests a saturation for the *p*-polarized THz component, which is much higher than that of InAs crystal, and a second-order nonlinear resonant optical rectification effect for the *s*-polarized THz component. Based on the nonlinear polarizability matrix of InAs, the calculated polarization angle dependence of the two THz components fit well with the experimentally obtained data. Moreover, the proportion of the second-order nonlinear optical effect in the *p*-polarized THz radiation mechanism of InAs NWs is  $\sim 15\%$ , much lower than the reported  $\sim 38\%$  of InAs crystal measured in reflection geometry. The enhancement of the linear transient photocurrent mechanism in InAs NWs could be induced by the localized surface plasmon resonance absorption of the In droplets because of the relatively matching radius range. This work clarifies the mechanisms of both the linear and nonlinear optical effect contribution for the THz generation in InAs NWs and paves the way for designing strong THz emitters with novel semiconductor structures.

## 2. Experimental Section

## 2.1 Sample preparation and characterizations

The InAs NW network was prepared on quartz substrate by a low-temperature NW growth mechanism, which was realized in an atmospheric pressure metalorganic vapor phase epitaxy system. The detail growth method can be found in the previous report [39, 40]. The self-catalyzed InAs NWs were grown from in situ deposited In particles. These metal particles could be conspicuous when the NWs are short, so the NWs look like a network of mushroom-shaped structures in this work. Morphology of the sample was studied using scanning electron microscope (SEM) (FEI Apreo S) and transmission electron microscope (TEM) (FEI Talos F200X). The elementary composition of the sample was measured by the energy-dispersive X-ray (EDX) spectroscopy that is integrated with the TEM system. The structural properties of the sample were tested using X-ray diffraction (XRD) (Bruker D8 Advance) spectroscopy.

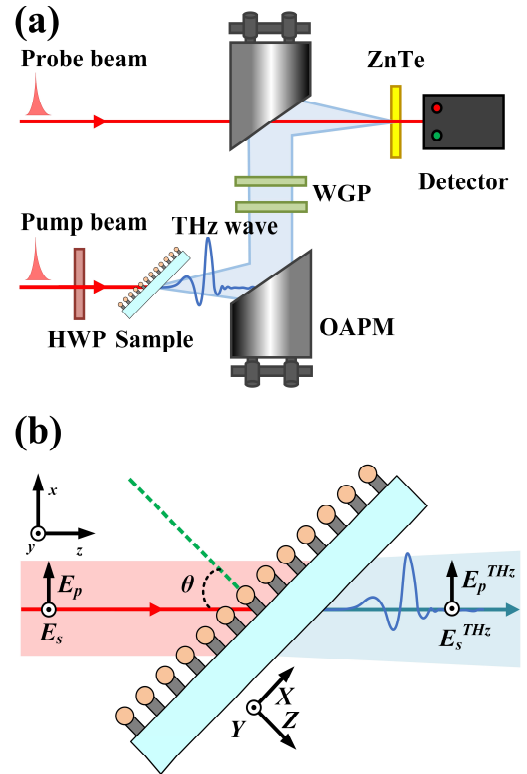
## 2.2 THz measurements

Figure 1a shows the schematic of the THz emission spectroscopy in a transmission configuration. A Ti:Sapphire regenerative amplifier system (800 nm central wavelength, 35 fs pulse duration, and 1 kHz repetition frequency) (Spectra-Physics, Spitfire) is used to output femtosecond pump pulses. The femtosecond laser beam is divided into a probe beam and a pump beam by a beam splitter. The laser beam shoots the sample with an incident angle ( $\theta$ ) of  $45^\circ$ . THz radiation generated from the InAs NW network is collected and collimated by a pair of off-axis parabolic mirrors (OAPM). The  $p$ -polarization and  $s$ -polarization components of the THz radiation can be extracted using a pair of wire-grid polarizer (WGP). A balanced detector is used to receive the detection beam passing through the detection crystal ZnTe (110). Figure 1b shows a schematic diagram of the THz generation process from the InAs NW network excited by the 800 nm femtosecond laser.  $E_p$  and  $E_s$  represent the  $p$ -polarization and  $s$ -polarization components of the pump laser, respectively.  $E_p^{THz}$  and  $E_s^{THz}$  represent the  $p$ -polarized and  $s$ -polarized components of THz radiation, respectively. The Cartesian coordinate system ( $xyz$ ) represents the laboratory coordinate system, and ( $XYZ$ ) represents the crystal coordinate system.

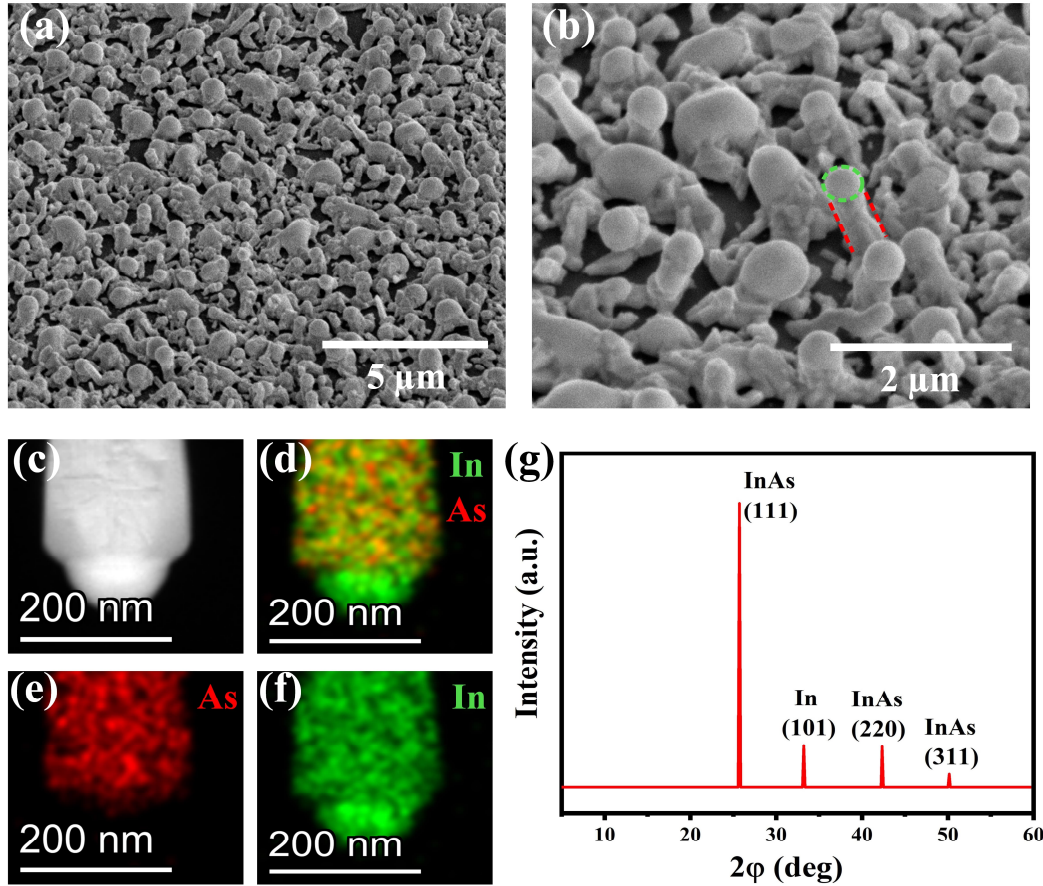
## 3. Results and Discussion

Figures 2a and 2b are the SEM images of the InAs NW network at different magnifications. Figure 2a shows uniformly distributed nanoscale integrated mushroom-shaped NWs grown on the quartz substrate. As illustrated in Figure 2b, the single NW consists of In droplet on the top and a short NW body on the bottom. The length of the NW is approximately  $0.8 \mu\text{m}$ , and the radius of the In droplet and

the NW are around 120 nm. Note that the radius values of different NWs have a relatively large variation range from  $\sim 80 \text{ nm}$  to  $\sim 200 \text{ nm}$ , and most of the NWs are distributed between  $\sim 100 \text{ nm}$  and  $160 \text{ nm}$ . Furthermore, we measured the TEM image (Figure 2c) of a single NW sample and analyzed the sample's elementary composition using Energy-dispersive X-ray spectroscopy (EDX). As shown in Figures 2d-2f, the NW part of the sample contains both In and As, while the In droplet part contains only In. This configuration is consistent with the reported element distribution of InAs NWs grown on Si [39]. Additionally, the X-ray analysis ( $2\varphi$ -scanning,  $\varphi$  is the scanning angle of the X-ray diffraction spectrometer) of the sample is performed via XRD. As shown in Figure 2g, there are three strong diffraction peaks at  $25.4^\circ$ ,  $42.1^\circ$ , and  $49.8^\circ$  positions, corresponding to the characteristic diffraction peaks of the (111), (220), and (311) crystal planes of InAs, respectively. These peaks suggest that InAs NWs have a zinc blende structure which belongs to the cubic crystal system with a space group of  $\bar{4}3m$ . Moreover, there is also a strong diffraction peak at the position where  $2\varphi$  is  $33^\circ$ , which corresponds to the characteristic diffraction peak of the (101) crystal plane of In. Therefore, the structural property of the InAs NW network has been confirmed.



**Figure 1.** (a) Schematic diagram of the experimental setup for THz emission spectroscopy measurement. (b) Schematic diagram of the THz generation process from the InAs NW network excited by the 800 nm femtosecond laser.



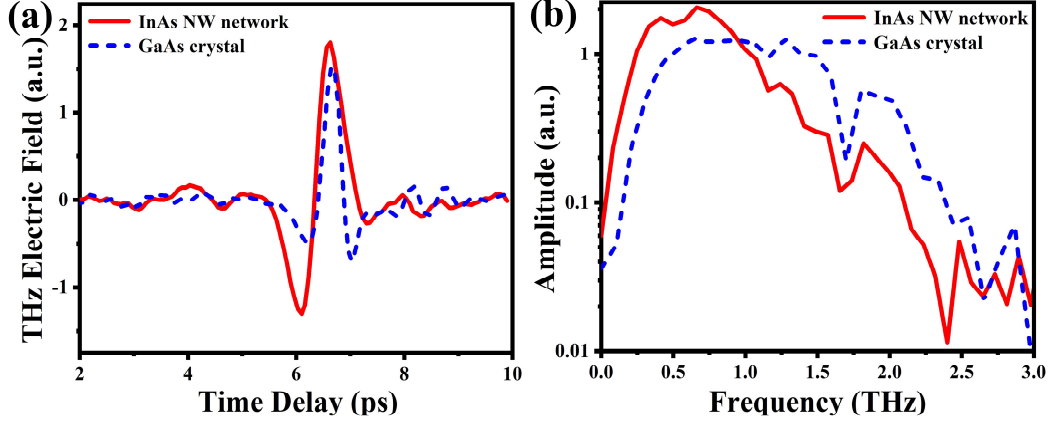
**Figure 2.** (a, b) SEM images of the mushroom-shaped InAs NW network with scale bars of 5  $\mu\text{m}$  and 2  $\mu\text{m}$  measured in bird's eyes view ( $45^\circ$ ). (c) TEM image of a single InAs NW measured with a 200 nm scale bar. (d-f) EDX spectra of the InAs NW network. Green and red regions represent the distributions of In and As, respectively. (g) XRD spectrum of the InAs NW network.

Figure 3a shows the THz emission time-domain spectra of the InAs NW network and a (100) GaAs crystal as a reference. The 800 nm excitation laser is *p*-polarized at an incident angle of  $45^\circ$ , and the pump fluence is 210  $\mu\text{J}/\text{cm}^2$ . The THz radiation electric fields of both InAs NW network and GaAs crystal show significant peak-to-valley waveforms. Here, GaAs crystal is a recognized THz emitter in traditional semiconductors used in transmission geometry. However, the InAs bulk crystals have no signal in the transmission geometry. The quartz substrate of the InAs NW network has no contributed to the THz emission [41]. Therefore, Figure 3a suggests that the THz signal generated by the InAs NW network has a larger peak-to-valley amplitude, which is approximately 1.5 times larger than that of the GaAs crystal, and has a little longer pulse duration of  $\sim 2$  ps. From the SEM results of the InAs NW network, the fill factor of NWs is low. Therefore, the THz emission efficiency of the InAs NW network is much larger than that of the GaAs crystal.

Figure 3b is the frequency-domain spectra processed by Fourier transformation. The results show that the InAs

NW network has a broadband THz emission spectrum from  $\sim 0.1$  to  $\sim 2.5$  THz. Moreover, the maximum THz amplitude of the InAs NW network is at  $\sim 0.75$  THz, which is lower than the frequency of GaAs crystal's maximum THz amplitude at  $\sim 1.3$  THz. The different frequency distribution of the THz signals from the InAs NW network and GaAs crystal could be attributed to the different THz generation mechanisms. In the following part, we study the THz generation mechanism of the InAs NW network by investigating multiple parameters.

Before analyzing the experimental data, the possible THz radiation mechanisms of the InAs NW network are discussed. The THz radiation mechanism under the ultrafast laser excitation can be related to the time derivative of the photogenerated carriers, the polarization, and the magnetization by the pump laser pulse [12]. Here, because both In and InAs are nonmagnetic, the magnetization-related mechanism could be excluded. In addition, the photon energy of 800 nm laser (1.55 eV) is much higher than the bandgap of InAs (0.36 eV), so the



**Figure 3.** THz emission spectra of InAs NW network and (100) GaAs crystal in the (a) time domain and (b) frequency domain.

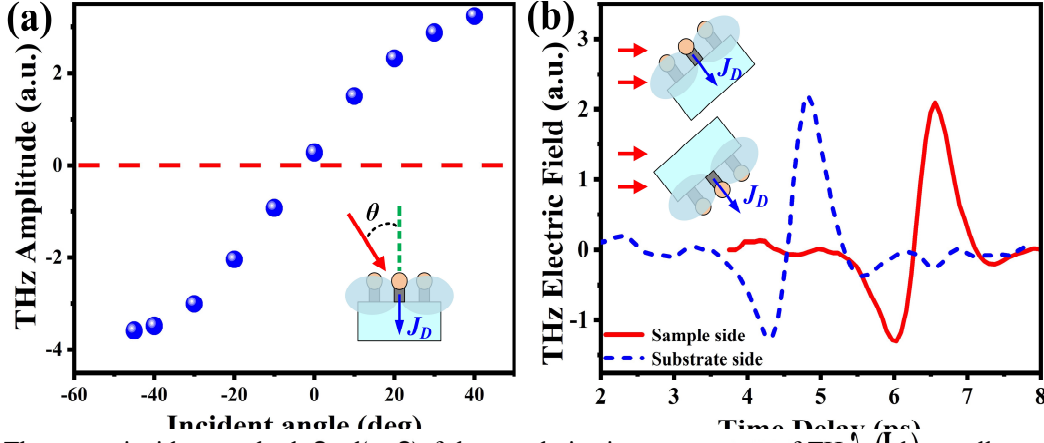
rapidly changing photogenerated carriers, namely transient photocurrent, could be the most probable source of the THz radiation. There can be linear and nonlinear optical mechanisms to accelerate the photogenerated carriers. The former is often related to the field with a constant direction, such as the surface depletion field, p-n junction field, and photo-Dember field [38, 42]. The latter could be caused by the resonant optical rectification effect (compared with optical rectification, resonant optical rectification excites real electron-hole pairs with above-bandgap absorptions, which can induce a shift current under linear polarization light excitation) [43] or the photon drag effect [44], both related to the nonlinear coefficient matrix of crystals.

Figure 4a shows the incident angle-dependent  $p$ -polarized peak-to-valley amplitude ( $E_p^{THz}$ ) of the THz signal emitted from the InAs NW network (negative values represent the polarity reversal of the time-domain pulse). Gradually enhanced absolute value of  $E_p^{THz}$  can be observed when the incident angle increases. Specifically, there is a small but non-zero value obtained at the normal incidence condition. Firstly, the variation tendency of the THz electric field at the non-zero angle is consistent with a dipole radiation model in which the dipole is along the Z-axis of the sample. This result suggests that a strong linear transient photocurrent  $J_D$  induced dipole radiation could exist in the sample, which has been illustrated in the inset of Figure 4a. Secondly, the non-zero THz radiation at normal incidence is not induced by the linear transient photocurrent but could be originated from a nonlinear optical effect, just like the similar phenomenon reported in MoS<sub>2</sub> crystal [45].

To narrow down the possible mechanisms, the THz time-domain signals generated by exciting the sample from the InAs side and the quartz substrate side are measured and shown in Figure 4b. Here, the two THz

pulses have similar waveform and amplitude. The time delay between the two pulses of  $\sim 2$  ps is induced by the different optical paths in the quartz substrate of the THz wave (the refractive index is  $\sim 1.955$  [46]) and the 800 nm laser (the refractive index is  $\sim 1.45$ ). In the nanoscale integrated mushroom-shaped InAs NW network, the interface is formed between the In particle and the upper end-face of InAs NWs. Two types of contact can be formed between metal and semiconductors: the Schottky contact and the Ohmic contact. According to the reported data, the work function of metal In is  $\sim 4.12$  eV [47], which is lower than the work function of InAs NWs of  $\sim 5.0$  eV [47]. Therefore, the contact between In and InAs should be Ohmic, as can be expected from the high doping level observed earlier in similar InAs NWs [40]. This conclusion can be supported by excluding the Schottky contact from the experiment result. If a Schottky contact is formed at the In/InAs interface, the direction of the transient photocurrent driven by the Schottky field should be inverted when changing the excitation side, thereby emitting THz pulses with reversed polarity [48, 49]. Ohmic contact does not provide a field that accelerates the carriers between In and InAs but an excellent carrier transport channel. Because metal In cannot generate THz wave under fs laser excitation, the origination of THz emission should be the InAs NWs. The In nanospheres could enhance the THz emission by increase the absorption of the nanostructure, which is discussed in the last part. Next, we investigate the specific THz emission mechanism of the InAs NWs.

Because the  $p$ -polarized and  $s$ -polarized THz components are induced by the different components of the transient photocurrent in the crystal coordinate system, we study the two THz components separately by changing the pump fluence and polarization angle. Figures 5a and 5b present the pump fluence dependence of the peak-to-



**Figure 4.** (a) The pump incident angle dependence of the  $p$ -polarization component of THz peak-to-valley amplitude. The inset illustrates the linear transient photocurrent mechanism of the THz generation. (b) THz time-domain signals generated by exciting the sample from the InAs side and the substrate side, which is also indicated in the inset.

valley amplitudes of the  $p$ -polarized THz component  $E_p^{THz}$  and the  $s$ -polarized THz component  $E_s^{THz}$ , respectively. For the  $E_p^{THz}$  component (Figure 5a), the THz amplitude increases with the pump fluence and approaches gradually to saturation at the high fluence region. The saturation phenomena have been observed in the linear ultrafast photocurrent induced THz emission such as in  $WS_2$  [50] and  $MoSe_2$  crystals [51] because the largely increased amount of photoexcited carriers could accumulate in the sample and induce an electrostatic shielding effect [45]. Here, the relationship between the pump fluence  $I_{pump}$  and the THz radiation amplitude  $E_{THz}$  can be described as [16]:

$$E_{THz} = SI_{pump} / (I_{pump} + I_{sat}), \quad (1)$$

Where  $S$  is a constant scaling factor, and  $I_{sat}$  the saturation intensity. From the red line in Figure 5a, Eq. (1) fits well with the experimental data of  $E_p^{THz}$ . Because the Schottky field has been excluded, surface depletion field and photo-Dember field could induce the transient photocurrent. Surface depletion field generally occurs in semiconductors with wide bandgaps such as GaAs and InP. In comparison, the photo-Dember effect is often active in narrow-bandgap semiconductors with a large difference between electron and hole mobility [38]. The THz generation mechanism in InAs crystal is verified to be photo-Dember effect [38, 52, 53] because of narrow bandgap of  $\sim 0.36$  eV and the significant difference between the electron mobility of  $30000 \text{ cm}^2 \text{ V}^{-1} \cdot \text{s}^{-1}$  and the hole mobility of  $240 \text{ cm}^2 \text{ V}^{-1} \cdot \text{s}^{-1}$  [54]. According to the reported THz emission works of InAs NWs, the photo-Dember effect is still the most possible mechanism for the THz generation phenomena [31-33]. However, we should note that the photo-Dember field in NWs is along the

axial direction due to the uneven illumination [31], different from the photo-Dember field formed perpendicular to the large-scale uniform surface of crystals. Moreover, the saturation intensity  $I_{sat}$  of our InAs NW network is calculated to be  $\sim 126 \mu\text{J}/\text{cm}^2$  from the fitting line in Figure 5a. For comparison, the THz emission from a (100) InAs crystal is measured in the reflection geometry, and the results are shown in Figure S1 in the Supporting Information. With the same excitation parameters, the saturation intensity of the InAs crystal is measured to be  $\sim 28 \mu\text{J}/\text{cm}^2$  (Figure S1b), which is much lower than that of the InAs NW network. The higher saturation intensity of the InAs NW network benefits from the unique NW structure, which reduces the electrostatic shielding effect induced by the photoexcited carrier accumulation. The structural advantage of the NW network is also the origination to make it as a transmission excitation available THz emitter, which cannot be realized with InAs crystal.

In comparison, the  $E_s^{THz}$  component of THz peak-to-valley amplitude increases linearly with pump fluence, as shown in Figure 5b. The linear dependence between the THz amplitude and pump fluence is related to a second-order nonlinear optical process which has been verified in materials such as  $MoS_2$  crystal [55],  $Bi_2Se_3$  crystal [56], and ultrathin gold films [57]. Here, the THz amplitude and the pump fluence have a relationship as [55]:

$$E_{THz} \propto \chi^{(2)} E_{(\omega)}^2 \propto I_{pump}, \quad (2)$$

Where  $\chi^{(2)}$  is the second-order nonlinear polarizability tensor,  $E_{(\omega)}$  the electric field of incident laser, and  $I_{pump}$  the pump fluence. From Figure 5b, the red line that calculated using Eq. (2) fits well with the experimental data. It suggests that the  $E_s^{THz}$  component of THz radiation from InAs NWs is due to a second-order nonlinear optical

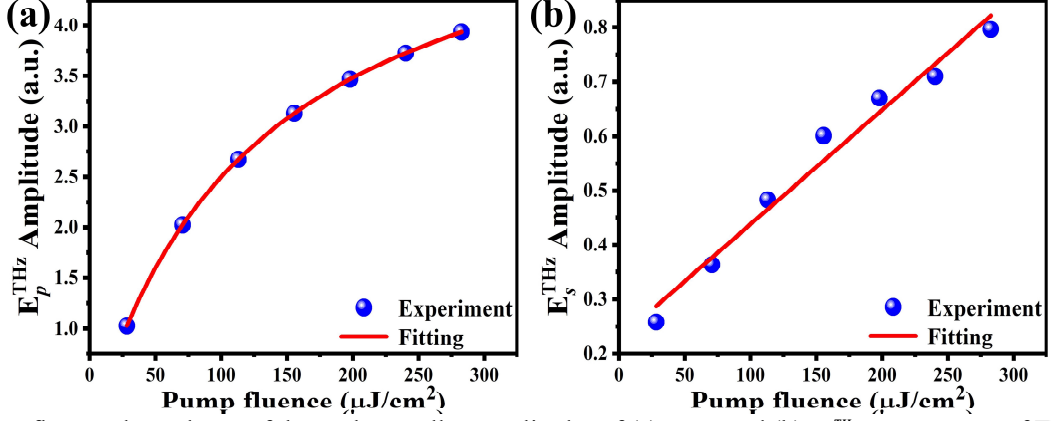


**Figure 5.** Pump fluence dependence of the peak-to-valley amplitudes of (a)  $E_p^{THz}$  and (b)  $E_s^{THz}$  components of THz radiation. Dots and lines represent the experimental and fitting results, respectively.

effect. Among the possible nonlinear photocurrent mechanisms, the photon drag effect can be excluded because it can induce a waveform polarity reversal, which has not been observed in this experiment. Therefore, the shift current induced by the resonant optical rectification effect, which is also the dominant nonlinear optical mechanism for the THz emission from InAs crystal, could be the mechanism for the  $E_s^{THz}$  component of THz generation from InAs NWs. This result provides clear experimental evidence for the nonlinear optical mechanism in the THz generation of InAs NWs.

To explore the different contributions of the linear and nonlinear photocurrents in the THz emission, the polarization angle dependence of the THz components is studied. Firstly, we should clarify the relationship between the THz components and the nonlinear optical effect induced transient photo-generated current components  $J_x$ ,  $J_y$ , and  $J_z$  ( $J_x$ ,  $J_y$ , and  $J_z$  represent the nonlinear transient photocurrents generated in  $X$ ,  $Y$ , and  $Z$  directions, respectively). According to the cardinal direction relations as shown in Figure 1b,  $E_p^{THz}$  and  $E_s^{THz}$  components of the generated THz radiation can be expressed as [58]:

$$E_p^{THz} \propto \frac{\partial J_z}{\partial t} \sin \theta_{THz} - \frac{\partial J_x}{\partial t} \cos \theta_{THz}, \quad (3)$$

$$E_s^{THz} \propto \frac{\partial J_y}{\partial t}, \quad (4)$$

Where  $\theta_{THz}$  is the refractive angle of the THz wave generated at the interface. When the incident angle is fixed, the  $p$ -polarized THz component is decided by  $J_z$  and  $J_x$ , and the  $s$ -polarized THz component is only dependent on  $J_y$ . Then, the polarization angle  $\alpha$  of the pump laser is related to the direction of the excitation laser electric field. Therefore, changing the polarization angle might induce different nonlinear photocurrent

component intensities due to the specific nonlinear polarizability matrix. However, polarization angle is independent of the linear photocurrent because the photo-Dember field has a fixed direction.

In the experiment, the polarization angle  $\alpha$  can be tuned from  $0^\circ$  to  $360^\circ$  by rotating the half-wave plate (HWP), the pump fluence is  $210 \mu\text{J}/\text{cm}^2$ , and the incident angle is  $45^\circ$ . Figures 6a and 6b show the polarization angle-dependent peak-to-valley amplitudes of  $E_p^{THz}$  and  $E_s^{THz}$  components, respectively. Both of the two components show a double rotation symmetry dependence on the polarization angle. For the  $E_p^{THz}$  component, there is a large DC offset of the oscillation. Because the DC offset is a polarization angle independent constant, it is caused by the linear photocurrent induced by the photo-Dember field along the axial direction of NWs. The linear photocurrent is denoted as  $J_D$  and illustrated in the inset of Figure 6a. Moreover, because the linear photocurrent only contributes to the  $Z$ -direction, the DC offset of the oscillation is very small in the  $E_s^{THz}$  component.

Then, we investigate the influence of the nonlinear optical effect. Here, the space group of InAs NWs is  $\bar{4}3m$  from the XRD spectrum. A calculation model of THz generation is established by referring to the process of second-harmonic generation (detailed calculation process can be found in the S1 part of Supporting Information). As a result, the polarization angle dependence of the THz radiation components can be written as:

$$E_p^{THz} \propto A \cos 2\alpha + B \sin 2\alpha, \quad (5)$$

$$E_s^{THz} \propto C \cos 2\alpha + D \sin 2\alpha, \quad (6)$$

Where  $A$ ,  $B$ ,  $C$ ,  $D$  are fitting constants, which are related to the nonlinear susceptibility of InAs NWs. Taking into account the contribution of the photo-Dember effect, the  $E_p^{THz}$  should become:

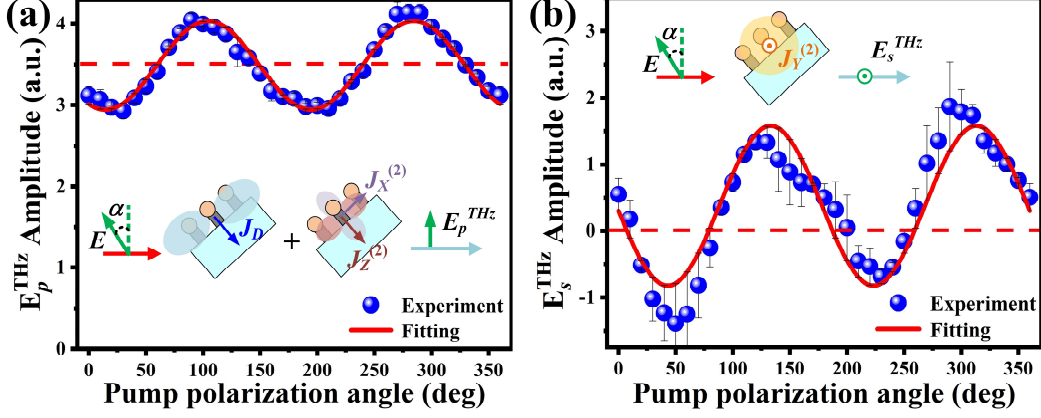


**Figure 6.** Pump polarization angle dependence of THz peak-to-valley amplitudes for (a)  $E_p^{THz}$  component and (b)  $E_s^{THz}$  component. Dots and lines represent experimental and fitting results, respectively. The insets illustrate the transient photocurrent mechanisms of the THz generation.

$$E_p^{THz} \propto A \cos 2\alpha + B \sin 2\alpha + K, \quad (7)$$

Where  $K$  is a constant in direct proportion to the THz radiation field generated by the photo-Dember effect. The red lines in Figures 6a and 6b are fitted with Eqs. (7) and Eq. (6), respectively. It suggests that the theoretical  $2\alpha$ -dependence agrees well with the experiment.

Based on the above discussion, the THz generation mechanisms for the  $E_p^{THz}$  component is a combination of linear and nonlinear transient photocurrent in  $X$ - and  $Z$ -directions (illustrated in the inset of Figure 6a), and the  $E_s^{THz}$  component is a nonlinear transient photocurrent in  $Y$ -direction (illustrated in the inset of Figure 6b). Moreover, the contribution of the nonlinear effect in  $E_p^{THz}$  is calculated to be  $\sim 15\%$ . For comparison, the polarization angle dependence of the  $p$ -polarized THz radiation from the (100) InAs crystal measured in the reflection geometry is also given in Figures S1c and S1d in Supporting Information. The contribution of the nonlinear optical effect in the InAs crystal is  $\sim 38\%$ . These results imply that the linear photocurrent induced THz radiation in InAs NW network is largely enhanced.

Here, we attribute the enhancement to the help of the localized surface plasmon resonance absorption of the In droplets. Localized surface plasmon resonance generally occurs in metal nanoparticles. Under the electric field of 800 nm pump laser, the free electrons on the surface of In droplets shift and deviate from the original equilibrium position. At the same time, the Coulomb force of the atomic nucleus will attract the offset electrons back to the equilibrium position. The combined force will eventually cause the electrons to reciprocate around the equilibrium position [59]. Using modified long-wavelength approximation, the absorption efficiency of In droplets with different radius has been calculated and shown in Figure S2 in Supporting Information. We have calculated the absorption cross section of In droplets with different radius.

When the radius rises from 100 to 160 nm, the resonant wavelength changes from  $\sim 700$  to  $\sim 1100$  nm. The optimal resonance enhancement for an 800 nm laser is obtained with a radius of  $\sim 112$  nm. Therefore, we believe it is the unique InAs NW network structure that accounts for the strong transmission THz emission comparable to GaAs from such a thin film with a thickness of only one micrometer. In addition, because THz generation is related to the NW length due to the surface effects that dominate the charge carrier transport properties as reported by Arlauskas *et al.* [32], enhanced THz emission could be expected when further increasing the length of NWs.

#### 4. Conclusions

Under the excitation of a linearly polarized femtosecond laser, the THz radiation from the mushroom-shaped InAs NW network is studied by changing several excitation parameters. From the THz signal's incident angle and direction dependence, the THz dipole radiation is deduced to have a fixed direction. The pump fluence dependence of the  $E_p^{THz}$  component is consistent with a linear transient photocurrent mechanism related to the photo-Dember field, and the saturation intensity of  $\sim 126 \mu\text{J}/\text{cm}^2$  is much larger than that of InAs crystal due to the advantage of one-dimensional structure. The linear relationship between the  $E_s^{THz}$  component and the pump fluence suggests a second-order nonlinear optical mechanism governed by the shift current. By analyzing the incident polarization angle dependence of the  $E_p^{THz}$  component, the proportion of second-order nonlinear optical effect in InAs NWs is calculated to be  $\sim 15\%$ , while that in InAs crystal is  $\sim 38\%$ . The enhanced THz emission from the linear transient photocurrent mechanism in InAs could be induced by the

resonant absorption of local plasma in the In droplets. This work clarifies that there is also a nonlinear optical mechanism in InAs NWs but contributes less than that in InAs crystal; the novel structure of the sample provides a valuable reference for the design of new powerful THz sources based on semiconductors.

## Acknowledgements

V.K. acknowledges the support of Aalto University Doctoral School, Walter Ahlström Foundation, Elektronikkainsinöörien Säätiö, Sähköinsinööriiliiton Säätiö, Nokia Foundation, Finnish Foundation for Technology Promotion (Tekniikan Edistämissäätiö) and Waldemar von Frenckell's foundation. H. Y. acknowledge the support from EU H2020-MSCA-RISE-872049 (IPN-Bio). We acknowledge the provision of facilities and technical support by Aalto University at Micronova Nanofabrication Centre.

## Funding

This work was supported by National Natural Science Foundation of China (No.: 11974279, 12074311, 11774288), Natural Science Foundation of Shaanxi Province (2019JC-25), Academy of Finland (No.: 314810, 333982, 336144 and 336818), Academy of Finland Flagship Programme (No.: 320167, PREIN), the European Union's Horizon 2020 research and innovation program (No.: 820423, S2QUIP; 965124, FEMTOCHIP), the EU H2020-MSCA-RISE-872049 (IPN-Bio), and ERC (834742).

## Data availability statement

All data that support the findings of this study are included within the article (and any supplementary files).

## References

- [1] Koenig S, Lopez-Diaz D, Antes J, Boes F, Henneberger R, Leuther A, Tessmann A, Schmogrow R, Hillerkuss D, Palmer R, Zwick T, Koos C, Freude W, Ambacher O, Leuthold J and Kallfass I 2013. Wireless sub-THz communication system with high data rate. *Nat. Photonics*, 7, 977-981.
- [2] Ma J, Shrestha R, Adelberg J, Yeh C Y, Hossain Z, Knightly E, Jornet J M and Mittleman D M 2018. Security and eavesdropping in terahertz wireless links. *Nature*, 563, 89-93.
- [3] Woodward R M, Cole B E, Wallace V P, Pye R J, Arnone D D, Linfield E H and Pepper M 2002. Terahertz pulse imaging in reflection geometry of human skin cancer and skin tissue. *Phys. Med. Biol.*, 47, 3853.
- [4] Zhang Y, Wang C, Huai B, Wang S and Zheng Y 2020. Continuous-Wave THz Imaging for Biomedical Samples. *Appl. Sci.*, 11, 71.
- [5] Mittleman D M and Jacobsen R H 1996. T-ray imaging. *IEEE J. Sel. Top. Quantum Electron.*, 2, P.679-692.
- [6] Federici J F, Schulkin B, Huang F, Gary D, Barat R, Oliveira F and Zimdars D 2005. THz imaging and sensing for security applications—explosives, weapons and drugs. *Semicond. Sci. Technol.*, 20, S266-S280.
- [7] He Y, Su R, Huang Y, Zhou Y, Zhao Q, Khurgin J B, Xiong Q and Xu X 2019. High-Order Shift Current Induced Terahertz Emission from Inorganic Cesium Bromine Lead Perovskite Engineered by Two-Photon Absorption. *Adv. Funct. Mater.*, 0, 1904694.
- [8] Zhou Y, Huang Y, Xu X, Fan Z, Khurgin J B and Xiong Q 2020. Nonlinear optical properties of halide perovskites and their applications. *Appl. Phys. Rev.*, 7, 041313.
- [9] Tong M, Hu Y, Xie X, Zhu X, Wang Z, Cheng X a and Jiang T 2020. Helicity-dependent THz emission induced by ultrafast spin photocurrent in nodal-line semimetal candidate Mg<sub>3</sub>Bi<sub>2</sub>. *Opto-Electronic Advances*, 3, 20002301-20002315.
- [10] Zhang X C and Auston D H 1992. Optoelectronic measurement of semiconductor surfaces and interfaces with femtosecond optics. *J. Appl. Phys.*, 71, 326-338.
- [11] Krotkus A 2010. Semiconductors for terahertz photonics applications. *J. Phys. D: Appl. Phys.*, 43, 273001.
- [12] Huang Y, Yao Z, He C, Zhu L, Zhang L, Bai J and Xu X 2019. Terahertz surface and interface emission spectroscopy for advanced materials. *J. Phys.: Condens. Matter*, 31, 153001.
- [13] Chang J, Wang H, Lei Z, Du W, Huang Y, Zhou Y, Zhu L and Xu X 2021. Coherent Elliptically Polarized Terahertz Wave Generation in WSe<sub>2</sub> by Linearly Polarized Femtosecond Laser Excitation. *J Phys Chem Lett*, 12, 10068-10078.
- [14] Zanotto L 2020. Single-pixel terahertz imaging: a review. *Opto-Electronic Advances*, 3, 200012.
- [15] McLaughlin R, Chen Q, Corchia A, Ciesla C M, Arnone D D, Zhang X C, Jones G A C, Linfield E H and Pepper M 2000. Enhanced coherent terahertz emission from indium arsenide. *J. Mod. Opt.*, 47, 1847-1856.
- [16] Reid M and Fedosejevs R 2005. Terahertz emission from (100) InAs surfaces at high excitation fluences. *Appl. Phys. Lett.*, 86, 011906.
- [17] Sarukura N, Ohtake H, Izumida S and Liu Z 1998. High average-power THz radiation from femtosecond laser-irradiated InAs in a magnetic field and its elliptical polarization characteristics. *J. Appl. Phys.*, 84, 654-656.
- [18] Ben-Zvi R, Bar-Elli O, Oron D and Joselevich E 2021. Polarity-dependent nonlinear optics of nanowires under electric field. *Nat Commun*, 12, 3286.
- [19] Kamiya K, Kayama K, Nobuoka M, Sakaguchi S, Sakurai T, Kawata M, Tsutsui Y, Suda M, Idesaki A, Koshikawa H, Sugimoto M, Lakshmi G, Avasthi D K and Seki S 2021. Ubiquitous organic molecule-based free-standing nanowires with ultra-high aspect ratios. *Nat Commun*, 12, 4025.
- [20] Kanne T, Marnauza M, Olsteins D, Carrad D J, Sestoft J E, de Bruijckere J, Zeng L, Johnson E, Olsson E, Grove-Rasmussen K and Nygard J 2021. Epitaxial Pb on InAs nanowires for quantum devices. *Nat Nanotechnol*, 16, 776-781.
- [21] Johnston M B, Whittaker D M, Corchia A, Davies A G and Linfield E H 2002. Simulation of terahertz generation at semiconductor surfaces. *Phys. Rev. B*, 65, 165301.
- [22] Trukhin V N, Bouravleuv A D, Mustafin I A, Kakkio J P, Huhtio T, Cirilin G E and Lipsanen H 2015. Generation of terahertz radiation in ordered arrays of GaAs nanowires. *Appl. Phys. Lett.*, 106, 252104.
- [23] Gyeong, Bok, Jung, Yong, Jae, Cho, Yoon, Myung, Han and Sung 2010. Geometry-dependent terahertz emission of silicon nanowires. *Opt. Express*, 18, 16353-9.
- [24] Lee W J, Ma J W, Bae J M, Jeong K S, Cho M H, Kang C and Wi J S 2013. Strongly enhanced THz emission caused by

- localized surface charges in semiconducting Germanium nanowires. *Sci. Rep.*, 3, 1984.
- [25] Park K, Min J-W, Subedi R C, Shakfa M K, Davaasuren B, Ng T K, Ooi B S, Kang C and Kim J 2020. THz behavior originates from different arrangements of coalescent GaN nanorods grown on Si (111) and Si (100) substrates. *Applied Surface Science*, 522.
- [26] Shin J H, Rhu H, Ji Y B, Oh S J and Lee W 2020. Anodically Induced Chemical Etching of GaAs Wafers for a GaAs Nanowire-Based Flexible Terahertz Wave Emitter. *ACS Appl Mater Interfaces*, 12, 50703-50712.
- [27] Peng K, Parkinson P, Boland J L, Gao Q, Wenas Y C, Davies C L, Li Z, Fu L, Johnston M B, Tan H H and Jagadish C 2016. Broadband Phase-Sensitive Single InP Nanowire Photoconductive Terahertz Detectors. *Nano Lett.*, 16, 4925-31.
- [28] Seifert P, Vaklinova K, Kern K, Burghard M and Holleitner A 2017. Surface State-Dominated Photoconduction and THz Generation in Topological Bi<sub>2</sub>Te<sub>2</sub>Se Nanowires. *Nano Lett.*, 17, 973-979.
- [29] Trukhin V N, Buyskih A C, Bouravlev A D, Mustafin I A, Samsonenko Y B, Trukhin A V, Cirlin G E, Kalitchevski M A, Zeze D A and Gallant A J 2015. Generation of terahertz radiation by AlGaAs nanowires. *JETP Lett.*, 102, 316-320.
- [30] Seletskiy D V, Hasselbeck M P, Cederberg J G, Katzenmeyer A, Toimil-Molaes M E, Léonard F, Talin A A and Sheik-Bahae M 2011. Efficient terahertz emission from InAs nanowires. *Phys. Rev. B*, 84, 115421.
- [31] Erhard N, Seifert P, Prechtel L, Hertenberger S, Karl H, Abstreiter G, Koblmüller G and Holleitner A W 2013. Ultrafast photocurrents and THz generation in single InAs nanowires. *Ann. Phys.*, 525, 180-188.
- [32] Arlauskas A, Treu J, Saller K, Beleckaite I, Koblmüller G and Krotkus A 2014. Strong terahertz emission and its origin from catalyst-free InAs nanowire arrays. *Nano Lett.*, 14, 1508-14.
- [33] Adomavičius R, Nevinskas I, Treu J, Xu X, Koblmüller G and Krotkus A 2020. Pulsed THz emission from wurtzite phase catalyst-free InAs nanowires. *J. Phys. D: Appl. Phys.*, 53, 19LT01.
- [34] Ramakrishnan G, Ramanandan G K, Adam A J, Xu M, Kumar N, Hendriks R W and Planken P C 2013. Enhanced terahertz emission by coherent optical absorption in ultrathin semiconductor films on metals. *Opt. Express*, 21, 16784-98.
- [35] Wu X, Quan B, Xu X, Hu F, Lu X, Gu C and Wang L 2013. Effect of inhomogeneity and plasmons on terahertz radiation from GaAs (100) surface coated with rough Au film. *Appl. Surf. Sci.*, 285, 853-857.
- [36] Berry C W, Wang N, Hashemi M R, Unlu M and Jarrahi M 2013. Significant performance enhancement in photoconductive terahertz optoelectronics by incorporating plasmonic contact electrodes. *Nat. Commun.*, 4, 1622.
- [37] Mendis R, Smith M L, Bignell L J, Vickers R E M and Lewis R A 2005. Strong terahertz emission from (100) p-type InAs. *J. Appl. Phys.*, 98, 126104.
- [38] Gu P, Tani M, Kono S, Sakai K and Zhang X C 2002. Study of terahertz radiation from InAs and InSb. *J. Appl. Phys.*, 91, 5533-5537.
- [39] Haggren T, Khayrudinov V, Dhaka V, Jiang H, Shah A, Kim M and Lipsanen H 2018. III-V nanowires on black silicon and low-temperature growth of self-catalyzed rectangular InAs NWs. *Sci. Rep.*, 8, 6410.
- [40] Khayrudinov V, Remennyi M, Raj V, Alekseev P, Matveev B, Lipsanen H and Haggren T 2020. Direct Growth of Light-Emitting III-V Nanowires on Flexible Plastic Substrates. *ACS Nano*, 14, 7484-7491.
- [41] Zhu L, Huang Y, Yao Z, Quan B, Zhang L, Li J, Gu C, Xu X and Ren Z 2017. Enhanced polarization-sensitive terahertz emission from vertically grown graphene by a dynamical photon drag effect. *Nanoscale*, 9, 10301-10311.
- [42] Yao Z, Zhu L, Huang Y, Zhang L, Du W, Lei Z, Soni A and Xu X 2018. Interface Properties Probed by Active THz Surface Emission in Graphene/SiO<sub>2</sub>/Si Heterostructures. *ACS Appl. Mater. Interfaces*, 10, 35599-35606.
- [43] Côté D, Laman N and van Driel H M 2002. Rectification and shift currents in GaAs. *Appl. Phys. Lett.*, 80, 905-907.
- [44] Obratsov P A, Kanda N, Konishi K, Kuwata-Gonokami M, Garnov S V, Obratsov A N and Svirko Y P 2014. Photon-drag-induced terahertz emission from graphene. *Phys. Rev. B*, 90, 241416.
- [45] Huang Y, Zhu L, Yao Z, Zhang L, He C, Zhao Q, Bai J and Xu X 2017. Terahertz Surface Emission from Layered MoS<sub>2</sub> Crystal: Competition between Surface Optical Rectification and Surface Photocurrent Surge. *J. Phys. Chem. C*, 122, 481-488.
- [46] Zhou Y, E Y, Ren Z, Fan H, Xu X, Zheng X, Yuan Lei D, Li W, Wang L and Bai J 2015. Solution-processable reduced graphene oxide films as broadband terahertz wave impedance matching layers. *J. Mater. Chem. C*, 3, 2548-2556.
- [47] Miao J, Hu W, Guo N, Lu Z, Zou X, Liao L, Shi S, Chen P, Fan Z and Ho J C 2014. Single InAs nanowire room-temperature near-infrared photodetectors. *ACS nano*, 8, 3628-3635.
- [48] Sakai K 2005. *Terahertz Optoelectronics*, Springer, Berlin.
- [49] Shi Y, Yang Y, Xu X, Ma S and Li W 2006. Ultrafast carrier dynamics in Au/GaAs interfaces studied by terahertz emission spectroscopy. *Appl. Phys. Lett.*, 88, 161109-161109-3.
- [50] Zhang L, Huang Y, Zhao Q, Zhu L, Yao Z, Zhou Y, Du W and Xu X 2017. Terahertz surface emission of d-band electrons from a layered tungsten disulfide crystal by the surface field. *Phys. Rev. B*, 96, 155202.
- [51] Fan Z, Xu M, Huang Y, Lei Z, Zheng L, Zhang Z, Zhao W, Zhou Y, Wang X, Xu X and Liu Z 2020. Terahertz Surface Emission from MoSe<sub>2</sub> at the Monolayer Limit. *ACS Appl. Mater. Interfaces*, 12, 48161-48169.
- [52] Chern G D, Readinger E D, Shen H, Wraback M, Gallinat C S, Koblmüller G and Speck J S 2006. Excitation wavelength dependence of terahertz emission from InN and InAs. *Appl. Phys. Lett.*, 89, 141115.
- [53] Reklaitis A 2010. Terahertz emission from InAs induced by photo-Dember effect: Hydrodynamic analysis and Monte Carlo simulations. *J. Appl. Phys.*, 108, 053102.
- [54] Gu P and Tani M 2006. *Terahertz Radiation from Semiconductor Surfaces*, Springer Berlin Heidelberg.
- [55] Huang Y, Zhu L, Zhao Q, Guo Y, Ren Z, Bai J and Xu X 2017. Surface Optical Rectification from Layered MoS<sub>2</sub> Crystal by THz Time-Domain Surface Emission Spectroscopy. *ACS Appl. Mater. Interfaces*, 9, 4956-4965.
- [56] Braun L, Mussler G, Hruban A, Konczykowski M, Schumann T, Wolf M, Munzenberg M, Perfetti L and Kampfrath T 2016. Ultrafast photocurrents at the surface of the three-dimensional topological insulator Bi<sub>2</sub>Se<sub>3</sub>. *Nat. Commun.*, 7, 13259.
- [57] Ramakrishnan G and Planken P C M 2011. Percolation-enhanced generation of terahertz pulses by optical rectification on ultrathin gold films. *Opt. Express*, 36, 2572-2574.

- [58] Johnston M B, Whittaker D M, Corchia A, Davies A G and Linfield E H 2002. Theory of magnetic-field enhancement of surface-field terahertz emission. *J. Appl. Phys.*, 91, 2104.
- [59] Jensen T, Kelly L, Lazarides A and Schatz G C 1999. Electrodynamics of Noble Metal Nanoparticles and Nanoparticle Clusters. *J. Cluster Sci.*, 10, 295-317.